2003

Spectral estimates of bed shear stress using suspended-sediment concentrations in a wave-current boundary layer

Guan-hong Lee
Virginia Institute of Marine Science

W. Brian Dade
Cambridge University

Carl T. Friedrichs
Virginia Institute of Marine Science, carl.friedrichs@vims.edu

Chris E. Vincent
University of East Anglia

Spectral estimates of bed shear stress using suspended-sediment concentrations in a wave-current boundary layer

Guan-Hong Lee[1] and W. Brian Dade[2]
Institute of Theoretical Geophysics, Cambridge University, Cambridge, UK

Carl T. Friedrichs
Virginia Institute of Marine Science, College of William and Mary, Gloucester Point, Virginia, USA

Chris E. Vincent
School of Environmental Sciences, University of East Anglia, Norwich, UK

Received 27 December 2001; revised 29 July 2002; accepted 11 February 2003; published 1 July 2003.

[1] High-resolution time series of suspended-sediment profiles have been obtained using an acoustic backscatter system at an inner shelf site (North Carolina) where flows are dominated by wind-driven currents and waves. We analyzed the spatial and temporal structure of near-bed turbulence in particle-transporting flows and scalar-like fluctuations of suspended-sediment concentrations. An important element of our analysis is a new inertial dissipation method for passive tracers to estimate the shear stress acting on the seabed, using the spectral properties of suspended sediment concentrations observed by acoustic backscatter sensors. In flows that provide adequate separation of the scales of turbulence production and dissipation, a sufficiently thick constant stress wall layer, and significant sediment suspension, frequency (or associated wave number) spectra of near-bed sediment concentration exhibit a $-5/3$ slope in the inertial subrange that spans frequencies of order 1 Hz. This observation suggests that the suspended sediment is effectively a passive tracer of turbulent fluid motions. Inversion of the relevant, Kolmogorov scaling equations yields estimates of the shear velocity that agree reasonably well with other, independent and widely used measures. High- and low-frequency limits on application of the inertial dissipation method to sediment concentration are related to the inertial response time of sediment particles and the sediment settling timescale. We propose that, in future applications, the inertial dissipation method for passive tracers can be used to estimate either the shear velocity, effective settling velocity of suspended sediment (or equivalent particle size) or dynamic bed roughness if two of these three quantities are independently known. *INDEX TERMS:* 4211 Oceanography: General: Benthic boundary layers; 4568 Oceanography: Physical: Turbulence, diffusion, and mixing processes; 4558 Oceanography: Physical: Sediment transport; *KEYWORDS:* turbulence, suspended sediment, inertial dissipation method, eddy diffusivity

Citation: Lee, G.-H., W. B. Dade, C. T. Friedrichs, and C. E. Vincent, Spectral estimates of bed shear stress using suspended-sediment concentrations in a wave-current boundary layer, *J. Geophys. Res.*, *108*(C7), 3208, doi:10.1029/2001JC001279, 2003.

1. Introduction

[2] The inner shelf comprises an important pathway for the wave- and current-driven transport of water, sediment and contaminants in nearshore marine environments. Here we examine a fundamental component of the transport processes at 13-m water depth in a micro-tidal environment where currents are predominantly wind-driven and interact with waves (Duck, North Carolina). Using data collected at the site during the fall of 1996, we analyze the spatial and temporal structure of near-bed turbulence in particle-transporting flows inferred from mean and fluctuating values of suspended-sediment concentration. An important element of our analysis is a new method to estimate the shear stress acting on the seabed, using the spectral properties of suspended sediment concentrations observed just above the bed.

[3] Our study is motivated by the recognition of Kolmogorov scaling in spectra of observed suspended-sediment concentrations, in which the spectral power (or variance) of suspended sediment concentration varies with frequency (or associated wave number) raised to the $-5/3$ power. *Soulsby et al.* [1984] observed and applied Kolmogorov spectral scaling of suspended sediment flux in a tidal current in ways

[1]Now at Korea Ocean Research and Development Institute, Ansan, South Korea.
[2]Now at Department of Earth Sciences, Dartmouth College, Hanover, New Hampshire, USA.

0148-0227/03/2001JC001279

similar to that described here. In this study, however, we consider measurements, acquired with a well-proven acoustic backscatter system (ABS), of suspended-sediment concentration in a wave-current boundary layer. Relative to open channel flow, wave-current boundary layers provide distinct challenges for the application of spectral scaling of turbulence because of the presence of intense oscillatory currents. Above the wave boundary layer, oscillatory currents can dominate advection of turbulence associated with mean stress, while within the wave boundary layer, waves generate instantaneous levels of turbulence which can greatly exceed the mean turbulence level above the wave boundary layer.

[4] An ABS, in contrast with earlier sampling technologies, provides the capability of noninvasively measuring suspended-sediment concentration profiles at high temporal (multiple Hz sampling frequencies) and spatial resolution (1-cm intervals). With such measurements, the understanding of boundary layer dynamics of sediment transport under currents and waves has improved over the last decade, particularly with respect to boundary conditions, mechanisms for sediment suspension, and vertical distribution of suspended sediment [e.g., *Vincent and Green*, 1990; *Hay and Bowen*, 1994; *Lee and Hanes*, 1996; *Traykovsky et al.*, 1999]. In this study, we exploit the advantages of ABS measurements to explore in detail the temporal and spatial characteristics of turbulence inferred from the spectra of suspended sediment concentrations. Moreover, we propose a new method, based on established relationships between the wave number of turbulent motions, turbulent kinetic energy of a flow, and the observed variance of passively transported suspended sediment, to estimate shear stress acting on the seabed.

[5] In the next section we present the key ideas about sediment transport by turbulence that underpin and motivate our approach. This is followed by a description of the field studies and a relevant analysis of the resulting observations of nearshore sediment transport by waves and currents. We conclude with a discussion of key findings and prospects for further work. A summary of the notation used in our analysis is given in section 7.

2. Analysis

2.1. Vertical Structure of Turbulent Eddy Diffusivity in Wave-Current Boundary Layers

[6] At the most fundamental level, many models of sediment transport by boundary layer flows (including those of inherently unsteady, wave-current boundary layers) consider particle-suspending turbulence as a diffusional process characterized by a time-averaged eddy diffusivity of magnitude K. Over sufficiently long times, this process is balanced by the tendency of individual particles to settle downward with average speed w_s. This balance can be expressed in terms of the time-averaged concentration of sediment C at elevation z above the bed by the expression

$$w_s C + K\partial C/\partial z = 0, \tag{1}$$

for which a lower boundary condition must be specified and is usually related to bed shear stress [e.g., *Smith*, 1977; *Sleath*, 1984; *Glenn and Grant*, 1987]. An important challenge introduced with equation (1) is the delineation of the vertical structure of the time-averaged eddy diffusivity in wave-current boundary layers. Several different closure schemes for such settings have been proposed [e.g., *Sleath*, 1990], but little effort has been made to resolve their general applicability under field conditions. Important exceptions include studies by *Vincent and Downing* [1994] who, by examining equation (1) with ABS data obtained in wave-current flows, inferred that eddy diffusivity increases linearly from the bed to about 20-cm elevation and decreases above that level. Subsequent studies in different settings have supported this view [*Sheng and Hay*, 1995; *Vincent and Osborne*, 1995; *Lee et al.*, 2002]. These findings are key to our subsequent application of the inertial dissipation method in that they support the presence of a bottom boundary layer, which is approximately 20-cm thick, with mean properties consistent with constant stress and the law of the wall.

[7] To further examine the structure of the wave-current boundary layer, we consider near-bed observations of sediment transport in the following terms. Upon rearrangement of equation (1) and introduction of the flow velocity scale u_* and wave-boundary layer length scale δ_w, we obtain a dimensionless measure of eddy diffusivity K_+ which can be evaluated directly from observations of suspended-sediment concentration and flow intensity in a wave-current boundary layer. This expression is given by

$$K_+ = -\frac{w_s}{\kappa u_*}\frac{C}{\Delta C}\frac{\Delta z}{\delta_w}, \tag{2}$$

where $\Delta C/\Delta z$ is the discrete gradient in sediment concentration evaluated at spatial intervals Δz, $\delta_w \equiv 2u_{*cw}/\omega$ is the thickness of the wave boundary layer associated with characteristic incident wave radian frequency ω [*Grant and Madsen*, 1986] (hereinafter referred to as GM), and $\kappa \equiv 0.4$ is von Karman's constant associated with the law of the wall (compare equation (3) below). Depending on the specific application, the generalized shear velocity, u_*, in equation (2) can be either u_{*cw}, the shear velocity characterizing the maximum bed stress induced by currents plus waves (GM), or u_{*c}, the shear velocity characterizing the mean stress above the wave boundary layer. Normalizing eddy diffusivity as indicated by equation (2) allows comparison of estimates of K made from observations in dynamically wide-ranging environments. In particular, if conditions of the simplest assumption of eddy diffusivity structure $K \sim \kappa u_* z$ are met, then there should be a one-to-one, linear relationship between K_+ and relative elevation, z/δ_w. The linear relationship should apply more closely using u_{*cw} or u_{*c} for u_* in equation (2) depending on whether waves or currents dominate sediment suspension at the height of the observations. Implicit in equation (2) is the assumption that the buoyancy effect due to sediment suspension is minimal. The validity of these assumptions, coupled with the notion that eddy diffusivities of mass and momentum are equivalent, underpin the following analysis.

2.2. Shear-Velocity Estimates From Measured Velocity Spectra

[8] The near-bed structure and intensity of turbulence control the dynamics of sediment transport in marine

boundary layers. A fundamental measure of boundary layer intensity is the mean shear stress τ_c imposed by a flow of fluid with density ρ on the seabed, and the associated shear velocity $u_{*c} \equiv (\tau_c/\rho)^{1/2}$ introduced in equation (2). Accordingly, several methods to infer values of τ_c and u_{*c} from flow measurements have evolved during the last several decades. The key elements of the most widely used techniques, along with their strengths and weaknesses, are reviewed by, among others, *Kim et al.* [2000] and *Dade et al.* [2001]. Among these techniques, the inertial dissipation method (hereinafter referred to as IDM) involves the use of spectra of the turbulent fluctuations to infer u_{*c} values. It is useful here to review the basis of this method as it is the starting point for a new approach to estimate bed shear stress from suspended sediment concentration and outlined in the next section.

[9] Dimensional considerations, coupled with the assumptions that shear stress τ_c is uniform in z and arises solely from turbulent fluid motions, requires that in the near-bed region of a boundary layer flow [e.g., *Tennekes and Lumley*, 1972; *Kundu*, 1990],

$$\partial u_c/\partial z = u_{*_c}/\kappa z \tag{3}$$

$$K\partial u_c/\partial z = u_{*_c}^2, \tag{4}$$

and hence

$$K = \kappa u_{*_c} z, \tag{5}$$

where u_c is current velocity averaged over wave and turbulent timescales. Equations (3)–(5) are related statements of the "law of the wall." These relations also assume that the fluid is unstratified and that any vertical density gradients due to the sediment suspension are dynamically negligible.

[10] In neutral, locally isotropic, horizontally homogeneous and stationary boundary layer flows there exists a range of eddy sizes over which turbulent kinetic energy (TKE) is transmitted to ever smaller scales and, ultimately, to viscous dissipation. The inertial subrange is defined as the domain of fluid motions over which the largest scales of turbulent energy production are well separated from those of viscous dissipation. Dimensional considerations require that this energy cascade on the inertial subrange results in a characteristic, three-dimensional TKE spectrum that can be described in terms of its spectral density $\phi_{ii}(k)$ (with units of $L^3\,T^{-2}$), rate of TKE dissipation ε ($L^2\,T^{-3}$), and eddy wave number k (L^{-1}), for which

$$\phi_{ii}(k) = \alpha_i \varepsilon^{2/3} k^{-5/3}, \tag{6}$$

where α_i is one dimensional Kolmogorov constant [*Tennekes and Lumley*, 1972]. In locally isotropic turbulence, $\alpha_1 \sim 0.51$ and $\alpha_2 = \alpha_3 = 4/3\alpha_1 \sim 0.69$ [*Huntley*, 1988; *Green*, 1992], where α_1 and α_2 are horizontal components parallel and transverse to the mean flow, respectively, and α_3 is vertical component.

[11] In practice, Eulerian estimates of TKE spectra are obtained as functions of frequency f (T^{-1}) rather than wave number k. Taylor's concept of "frozen turbulence" [e.g., *Tennekes and Lumley*, 1972] specifies that

$$\phi_{ii}(k) = U\phi_{ii}(f)/2\pi, \tag{7}$$

where U is the dominant flow speed characteristic of frequencies below the spectrum of interest. Equation (7) holds if the characteristic lifetimes of turbulent eddies can be reasonably assumed to be much larger than the characteristic time required for eddies to advect past the point or, equivalently, if

$$k\phi_{ii}(k)/U^2 \ll 1. \tag{8}$$

Introduction of equation (7) and $k = 2\pi f/U$ into equation (6) with subsequent rearrangement yield an expression for TKE frequency spectra given by

$$\phi_{ii}(f) = \alpha_i(\varepsilon U/2\pi)^{2/3} f^{-5/3}. \tag{9}$$

Despite the seemingly restrictive assumptions underlying the derivation of equations (6) and (9), a range of wave numbers or equivalent frequencies over which TKE spectra exhibit Kolmogorov scaling has been demonstrated in many benthic boundary layers [e.g., *Gross and Nowell*, 1985; *Huntley*, 1988; *Green*, 1992].

[12] Within the inertial subrange, and in the absence of any other sources or sinks of energy, the rates of turbulent kinetic energy (TKE) production by mean-flow shear acting on turbulent eddies of intensity u_{*c} and dissipation ε by viscosity must be in balance. The balance between rates of TKE production and dissipation can be expressed in terms of the mean-flow gradient $\partial u_c/\partial z$ and the shear velocity u_{*c} as

$$\varepsilon = u_{*_c}^2 \partial u_c/\partial z = K(\partial u_c/\partial z)^2. \tag{10}$$

The relationships introduced in equations (3)–(5) and (10) jointly require that

$$\varepsilon = u_{*_c}^3/\kappa z. \tag{11}$$

Substitution of this result into equation (6) or (9) and subsequent rearrangement yield, respectively,

$$u_{*_c} = \left[\alpha_i^{-1} k^{5/3} \phi_{ii}(k)(\kappa z)^{2/3}\right]^{1/2}, \tag{12}$$

or

$$u_{*_c} = \left[\alpha_i^{-1} f^{5/3} \phi_{ii}(f)(2\pi\kappa z/U)^{2/3}\right]^{1/2}. \tag{13}$$

Thus, an estimate of u_{*c} can be obtained from spectral analysis of a boundary layer flow observed at a known elevation z.

[13] A potentially important complication addressed by *Huntley* [1988] is that equations (6)–(13) will not be valid unless two conditions are met. First, the measurements must be made within the constant stress layer. Second, a critical Reynolds number,

$$Re_{cr} = \kappa u_{*_c} z/\nu, \tag{14}$$

must be exceeded to ensure separation between turbulence production and dissipation, where ν is the kinematic viscosity of the ambient fluid and $2500 < Re_{cr} < 4000$. The corresponding critical height, z_{cr}, above which measurements must be made to ensure an inertial subrange is then

$$z_{cr} = Re_{cr}\nu/(\kappa u_{*_c}). \quad (15)$$

Huntley developed an empirical formula to correct shear-velocity estimates obtained from equation (12) or (13) for elevations less than z_{cr}. This correction is given by

$$\hat{u}_{*_c} = \left(Re_{cr}u_{*_c}^3\nu/\kappa z\right)^{1/4}, \quad (16)$$

where u_{*_c} is the uncorrected estimate from equation (12) or (13), and $\hat{u}_{*_c}$ is a new estimate corrected for the effects of subcritical elevation. In our calculations, we set $Re_{cr} = 3000$ [*Huntley*, 1988]. The physical significance of equation (16) is not well understood, but its essential role in useful estimates of bed shear stress in many, diverse settings is widely recognized [e.g., *Huntley*, 1988; *Green*, 1992; *Kim et al.*, 2000].

2.3. A New Method of Estimating the Shear Velocity From Sediment Concentration Time Series

[14] Scalar quantities, such as measures of the concentration of heat, solutes or other passive tracers, exhibit a similar distribution of spectral density over an inertial subrange of wave numbers or equivalent frequencies in well-developed turbulent flows [*Tennekes and Lumley*, 1972]. By taking the analogy between temperature and suspended sediment measured in units of concentration Ψ, dimensional considerations yield general relationships analogous to that introduced in equation (6) given by

$$\phi_s(k) = \alpha_s\varepsilon_s\varepsilon^{-1/3}k^{-5/3}, \quad (17)$$

or, equivalently, in terms of frequency spectra by the concept of frozen turbulence (compare equation (7)),

$$\phi_s(f) = \alpha_s\varepsilon_s\varepsilon^{-1/3}(U/2\pi)^{2/3}f^{-5/3}, \quad (18)$$

where $\phi_s(k)$ and $\phi_s(f)$ represent the spectral energy density of sediment concentration (with units of either Ψ^2L or Ψ^2T, respectively), ε_s (Ψ^2T^{-1}) is the rate of dissipation of fluctuating sediment concentration, and α_s is an empirical constant pertaining to the class of scalars of interest. Equations (17) and (18) are well established for heat and solutes in atmospheric and marine boundary layers for which $\alpha_s = 0.71$ [*Hicks and Dyer*, 1972; *McPhee*, 1998; *Sharples et al.*, 2001]. *Soulsby et al.* [1984] noted the similarity of equations (9) and (18) when applied to coincident records of velocity and suspended sediment concentration in a tidal flow. Here we extend the analysis of *Soulsby et al.* [1984] by incorporating the sediment diffusion equation to solve for shear velocity. We end this section with a discussion of theoretical limitations of applying IDM to suspended sediment concentration in wave-current boundary layers.

[15] Assuming a local balance between the production of concentration variance and its dissipation, the dissipation rate ε_s of turbulence-driven fluctuations in scalar concentration C introduced in equations (17) and (18) is given by [e.g., *Hicks and Dyer*, 1972; *Soulsby et al.*, 1984; *McPhee*, 1998; *Sharples et al.*, 2001]

$$\varepsilon_s = -\overline{w'c'}\frac{\partial C}{\partial z}, \quad (19)$$

where c' is the fluctuating part of the tracer concentration. Additionally, the vertical, turbulent flux of sediment is assumed to be well-described in terms of eddy diffusivity for which

$$\overline{w'c'} = -K\frac{\partial C}{\partial z}, \quad (20)$$

where eddy diffusivity is taken to be equal to eddy viscosity. In the case of a steady and horizontally uniform distribution of suspended sediment described by the time-averaged sediment diffusion equation (1),

$$\partial C/\partial z = -w_s C/K, \quad (21)$$

and thus

$$\varepsilon_s = (w_s C)^2/\kappa u_{*_c} z. \quad (22)$$

Substitution of equations (11) and (22) into equations (17) and (18) and subsequent rearrangement of the result to isolate the shear velocity u_{*_c} yields, respectively,

$$u_{*_c} = (w_s C)\left[\alpha_s\{\phi_s(k)\}^{-1}k^{-5/3}(\kappa z)^{-2/3}\right]^{1/2} \quad (23)$$

and

$$u_{*_c} = (w_s C)\left[\alpha_s\{\phi_s(f)\}^{-1}f^{-5/3}\,(U/2\pi\kappa z)^{2/3}\right]^{1/2}. \quad (24)$$

Note that there is a dependence on elevation z in equations (23) and (24) not present in the analogous expressions for spectral estimates based on turbulence in equations (12) and (13). This difference accommodates nonuniform turbulent flux of sediment. The analogous constraint for turbulence spectral estimates, which eliminates z-dependence, is uniform stress in the near-bed region.

[16] Although temperature is a property of the fluid while sediment suspension is essentially a two-phase system, there are both theoretical [*Snyder and Lumley*, 1971; *Lumley*, 1977] and experimental [*Smith and McLean*, 1977; *Soulsby et al.*, 1984; *Glenn and Grant*, 1987] grounds for making this analogy under certain conditions. For the turbulent motion of a suspended particle to be indistinguishable from that of the surrounding fluid, key ratios must be satisfied regarding the particle's (1) size, (2) inertia and (3) settling trajectory [*Snyder and Lumley*, 1971]. First, the particle diameter, d, must be small relative to the smallest length scale of fluid motion, known as the Kolmogorov microscale $(\nu^3/\varepsilon)^{1/4}$, where ν is kinematic viscosity ($\approx 0.01 cm^2/s$ for seawater). If $d \geq (\nu^3/\varepsilon)^{1/4}$, distinct velocities will act on various portions of the particle. Second, the particle's inertial response time, as scaled by w_s/g, where g is the acceleration of gravity (≈ 980 cm/s^2), must be much smaller than the Kolmogorov

time microscale, $(\nu/\varepsilon)^{1/2}$. If $w_s/g \geq (\nu/\varepsilon)^{1/2}$, then the particle will not respond to small scale temporal changes in velocity as quickly as the fluid itself. Finally, the sediment fall velocity must be small relative to the turbulent velocity ($\sim u_*$), or the particle will fall from one eddy to another more quickly than the fluid is passed among eddies.

[17] The two constraints related to the Kolmogorov microscale limit the ability of suspended particle motion to represent turbulent fluid velocity at very short time and length scales. If $d > (\nu^3/\varepsilon)^{1/4}$ and/or $w_s/g > (\nu/\varepsilon)^{1/2}$, then the smallest velocity and timescales potentially resolved by observations of sediment motion will be of order d and w_s/g, even if these are not the smallest turbulent scales. For fine sand, these inherent resolution limits ($d = \sim 100$–300 μm, $w_s/g = \sim 1$–3 ms) are smaller than the smallest scales typically used in the inertial dissipation method when evaluating $-5/3$ spectra of velocity or passive tracers in the ocean. In the extreme of $w_s \gg u_*$, violating the third constraint above causes a settling particle to experience a frozen turbulence field as it rapidly cuts through the fluid turbulence [*Snyder and Lumley*, 1971]. This causes the autocorrelation of the turbulence seen by the particle to deviate from the true Lagrangian autocorrelation of the fluid turbulence. As long as the mean fall velocity is uncorrelated to the turbulent field, however, the net effect of the settling trajectory on the $-5/3$ method applied to small scales is consistent with the frozen turbulence assumption used to translate $\phi(k)$ to $\phi(f)$ for any tracer. The additional error at short time and space scales associated with neglecting w_s is then $O(w_s/U)$ and is relatively small.

[18] Practically, however, the condition $w_s > u_*$, can still be problematic because (1) relatively little sediment may be in suspension, undermining the assumption of a continuous field, and (2) individual particles put into suspension will remain there for only a short while. For $w_s > u_*$, the typical suspension timescale is only on the order of δ_s/w_s, where δ_s is a characteristic suspension height. If δ_s corresponds to the height of the constant stress layer, approximately 20 cm, for example, then the upper limit for turbulent timescales well-represented by 200 μm sand will be on the order of 10 s. We accordingly limit applications of sediment concentration IDM to (1) bursts with significant suspension and (2) frequencies above w_s/δ_s.

[19] Given the above restrictions, we do not expect the inherent decoupling of suspended sediment from fluid turbulence to further limit application of the $-5/3$ method. However, IDM may still be undermined by the same conditions which apply to any tracer of turbulence: (1) Measurements must be made within a steady, spatially uniform, unstratified constant stress layer; (2) sufficient separation must exist in the inertial subrange between the scales of turbulence production and dissipation; and (3) the characteristic lifetimes of turbulent eddies in the inertial subrange must be much larger than the characteristic time required for eddies to advect past the point of Eulerian measurement.

2.4. Summary of Analysis

[20] In this section we have reviewed existing and new ideas about sediment transport in the sea. In equation (2) we introduce a dimensionless form of eddy diffusivity K that can be used to test the relevance of the law of the wall analog to observations of suspended-sediment concentrations in wave-current boundary layers with wide-ranging dynamics. Equations (6)–(9) and (17)–(18) state the Kolmogorov scaling relationships between the spectral distribution of variance and wave number or frequency for time series observations of boundary layer flow velocities and passive concentrations, respectively. The scaling relationships for flow velocity given by equations (6)–(9), in particular, are the basis of well-proven expressions, given by equations (12) and (13), for estimating a fundamental measure of boundary layer flow intensity, the shear velocity u_*.

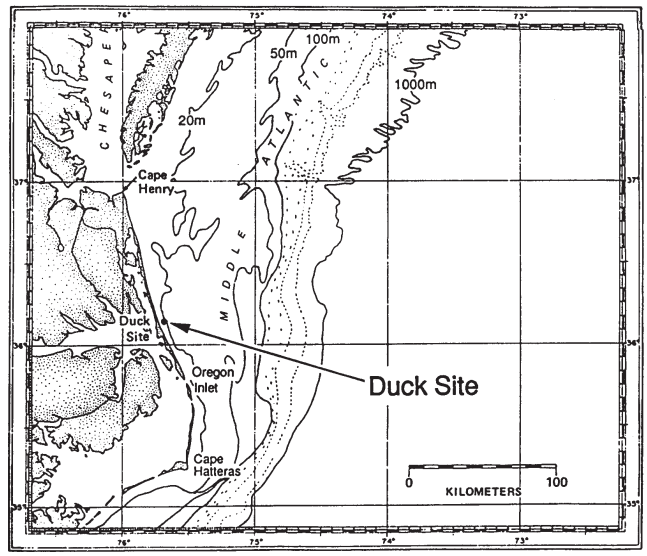

Figure 1. Location map of Duck site. VIMS tripod was deployed at a depth of about 13 m off the Field Research Facility, Duck, North Carolina.

[21] In equations (19)–(24), we advance a new method for evaluating u_{*c} based on the scaling relationships relevant to suspended-sediment concentration spectra as indicated in equations (17) and (18). Notable requirements for meaningful application of equations (19)–(24) include (1) significant sediment suspension, and (2) turbulent timescales that fall within the range $[w_s/g, \delta_s/w_s]$. In the following section, we describe a field experiment that validates these ideas.

3. Field Study

[22] Observations of flow conditions and sediment concentration were made during October 1996 at 13-m depth at Duck, North Carolina. This site is dominated by wind-driven currents and waves, and exhibits relatively simple, planar bathymetry (Figure 1). Tides are semidiurnal with a mean range of approximately 1 m (spring tide range ~ 1–2 m). Wave energy is usually relatively high during the winter months and relatively low during spring and summer. The mean current generally flows to the north in summer months and southward during winter, but short-lived reversals of flow direction are common. Storms are usually associated with extratropical northeasters during autumn, winter and early spring, and occasionally with tropical storms and hurricanes during late summer and autumn. *Birkemeier et al.* [1985] provide a more detailed description of the site. Surficial bottom sediments at the Duck site are moderately well sorted, range from medium to fine sand, and

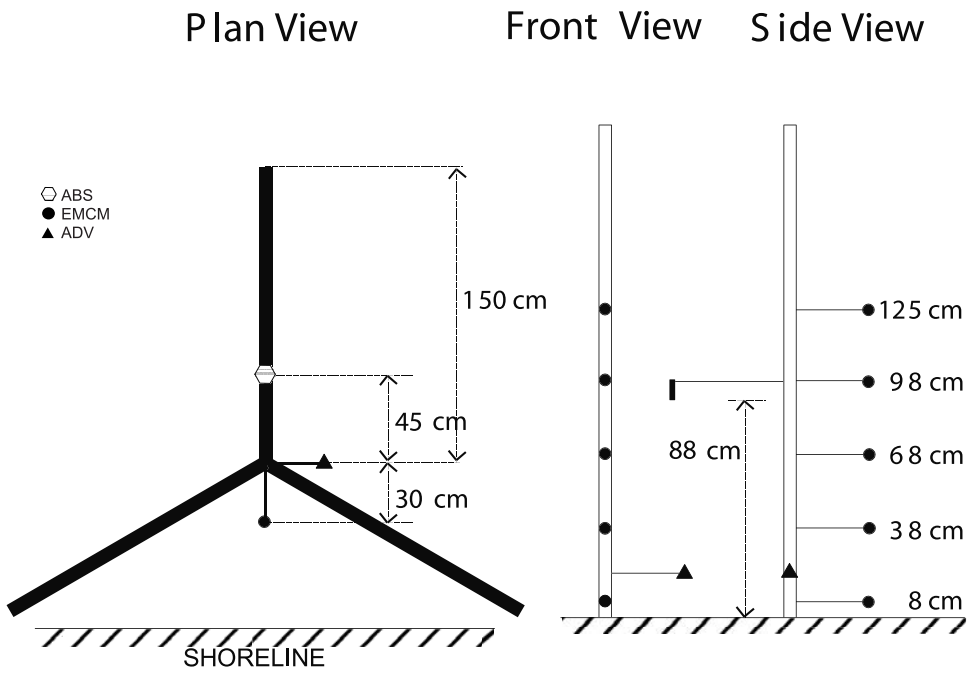

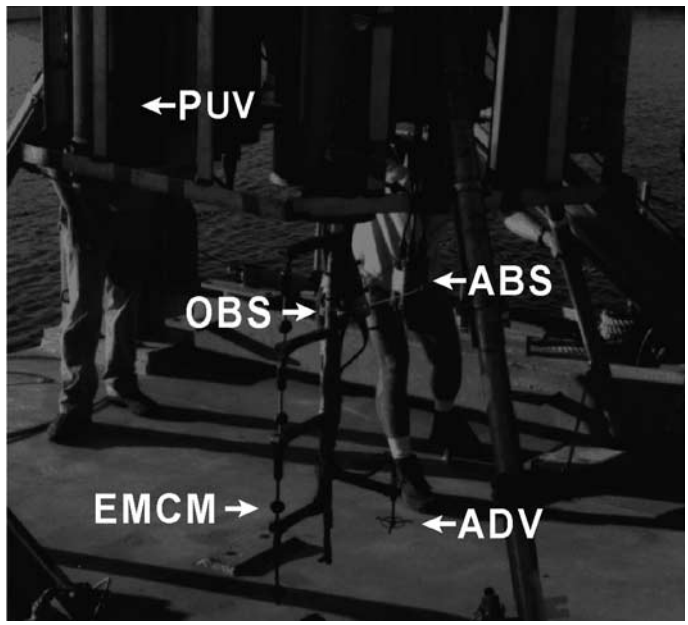

Figure 2. Plan view of VIMS tripod and configuration of instruments.

volumetrically comprise silts and clays to less than 10 percent [*Lee et al.*, 2002]. The median size, d_s, of sediment in samples collected by divers is 0.012 cm, for which the relative excess density s = 1.65, the settling velocity w_s = 1.0 cm/s in seawater of characteristic density and viscosity [*Dietrichs*, 1982]. Divers' observations indicate that at the time of deployment the seabed was weakly rippled.

[23] Instrumentation deployed at Duck included five electromagnetic current meters (EMCMs), at initial heights of 8-, 38-, 68-, 98- and 125-cm above the bottom (ab), one pressure sensor (at 195-cm ab), three transceiver ABSs (all 88-cm ab) and one acoustic Doppler velocimeter (ADV; 19-cm ab) (Figure 2) [*Lee et al.*, 2002]. A sediment trap was mounted on a leg of the deployment frame 100-cm ab. The EMCMs and pressure sensor recorded data at 1 Hz in bursts of 34-min duration every 2 hours, while the ABS and ADV recorded data at 5 Hz in 12-min bursts at 2-hour intervals. The data were recorded in self-contained data loggers. Optical backscatter sensors (OBS) were deployed but, owing to severe fouling, yielded poor data. Accordingly, these data are not considered.

[24] During the deployment in autumn 1996, the site was subject to extratropical storm conditions. Shown in Figure 3 are time series of environmental conditions including mean

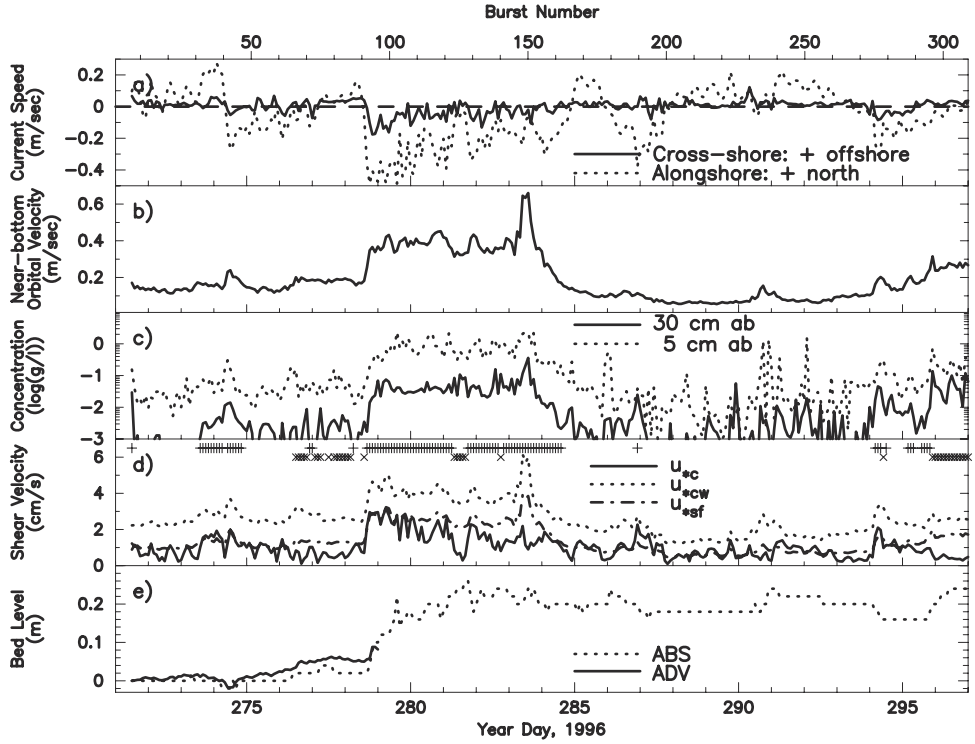

Figure 3. Environmental conditions during VIMS tripod deployment. (a) Along- and cross-shore current velocity observed at about 1 m ab; (b) near-bed wave orbital velocity; (c) observed concentrations at 5 (solid line) and 30 (dotted line) cm ab; (d) shear velocity. The periods that $u_{*sf,gm} > u_{*cr}$ and $R < 1$ (strong currents) are shown with plus, while the periods that $u_{*sf,gm} > u_{*cr}$ and $R > 1$ (weak currents) are shown with a cross; (e) bed level change observed by ADV and ABS.

flow at approximately 100-cm ab, near-bed wave orbital velocity, shear velocities ($u_{*sf,gm}$, $u_{*cw,gm}$ and $u_{*c,gm}$) and bed level relative to that observed at the onset of measurement. Throughout this paper, the first subscript on u_* indicates the type of shear velocity under consideration, and the second subscript (if any) represents the estimation method. Skin-friction shear velocity (u_{*sf}) isolates the component of shear stress responsible for mobilization of sediment at the bed. In contrast, u_{*cw} and u_{*c} are measures of the turbulence strength responsible for sediment diffusion within the wave boundary layer and overlying current boundary layer. The shear velocities and thickness of wave boundary layer displayed in Figure 3 were estimated by applying the GM wave-current interaction model as described by *Lee et al.* [2002].

[25] The ABSs were calibrated in a specially designed, laboratory tank at the University of East Anglia using a mixture of sand collected in the sediment trap during the experiment and sand taken from the bottom by divers at the beginning of the experiment. The backscatter signals at 54-cm below the three ABS transducers were inverted to obtain suspended sediment concentration. Figure 4 shows the comparison of ABS measurement and suction samples at 54 cm below the transducer. The lowest calibrated concentration was approximately 0.04 g/L. Since the backscattered pressure from a particle in the beam of the ABS transceiver is inversely proportional to the range from the transducer and the mass concentration is proportional to the backscattered pressure squared [*Thorne et al.*, 1993],

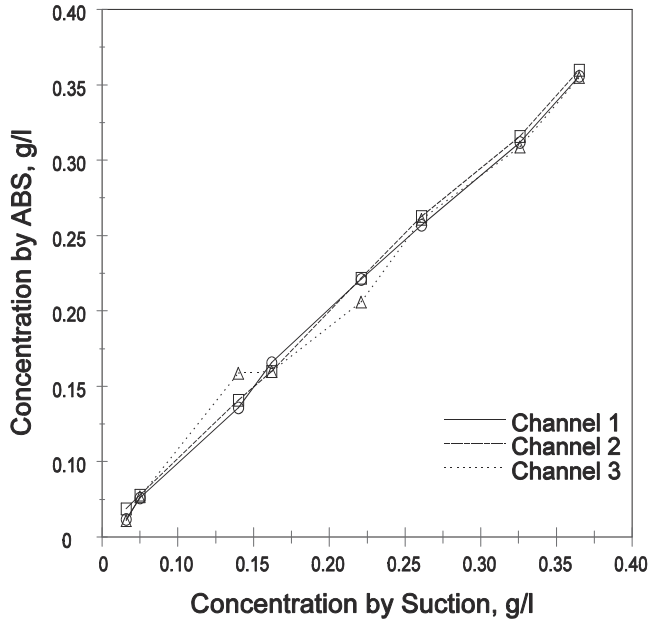

Figure 4. Comparison of concentrations by sand suction and ABS measurement in the UEA calibration tank at a distance of 54 cm from the ABS transducers. Figure is reprinted from *Lee et al.* [2002].

the accuracy of the ABSs corresponds to ~0.005 g/L at a distance of 20 cm from the transducer.

4. Data Analysis

[26] The following analysis was applied to ADV data (sampling bursts 1–90) recorded before the onset of a storm in early October 1996 (calendar day 279), after which the reliability of the ADV data came into question owing to sensor proximity (to within 3 cm) to an accreting bed. Errors in near-bed flow measurements associated with bed proximity have been noted elsewhere and attributed to significant increases in random motion of scattering targets and mean velocity shear within the sampling volume [*Voulgaris and Trowbridge*, 1998]. For bursts 1–90 the ADV sampling volume was an average distance of 16.5 cm from the bed. Although all 309 bursts of ABS data were analyzed, results of ABS data analysis are only presented for bursts where energy conditions were sufficient to suspend sand. The critical condition is determined as $u_{*sf,gm} > u_{*cr}$ (critical shear velocity for initiation of motion) because for median grain size (120 μm) of bed sediment at Duck critical shear velocity for initiation of motion (u_{*cr} = 1.22 cm/s) is greater than critical shear velocity for suspension (w_s = 1.01 cm/s). During the period of $u_{*sf,gm} > u_{*cr}$, concentration at 30 cm ab in general exceeds the calibrated ABS accuracy, 0.005 g/l (Figure 3). These bursts are indicated in Figure 3d.

[27] Standard transformations of time series observations of flow velocities and suspended sediment concentrations were used to obtain their Fourier spectra [e.g., *Bendat and Piersol*, 1986]. Original time series of velocities and ABS concentration measurements comprised 3072 and 2048 records, respectively, and, following conventional prewhitening of the series, were partitioned into segments of equal length (each 512 records) and with 50 percent overlap with adjoining segments. A Hanning window was applied to each segment before Fourier transformation. The resulting spectra were arithmetically averaged, thus the 95 percent confidence intervals correspond to 0.61–1.94 times and 0.54–2.48 times the smoothed spectral estimates of velocity and concentration data, respectively. The resulting estimates of u_{*c} are proportional to the square root of the power density of the velocity and concentration spectra. At the 95 percent confidence level, therefore, uncertainty on estimates at each frequency amounts to approximately 40 percent and 60 percent for flow- and sediment-spectral values, respectively. Standard errors of u_{*c} estimates, obtained by averaging over an inertial subrange of frequencies, amount to no more than about 10 percent of the reported values. The criteria used to identify the inertial subranges are described below.

[28] The inertial dissipation method has been criticized as unreliable in wave-dominated environments because wave orbital velocities can confound the computation of the turbulent-velocity spectrum [*Lumley and Terray*, 1983; *Gross et al.*, 1994; *Trowbridge*, 1998; *Shaw et al.*, 2001]. Analysis methods to minimize the effect of waves have been introduced with mixed results [*Lumley and Terray*, 1983; *Green*, 1992; *Gross et al.*, 1994]. However, it should be realized that the kinematic effect of superimposing waves does not necessarily imply a dynamic effect on the energy cascade. Shown in Figure 5 is an example of spectral density of flow velocity during conditions of moderate wave energy. Note that the spectra of the horizontal velocity components u and v exhibit the effects of wave energy, but that the vertical velocity component w does so, if at all, to a much lesser degree [cf. *Stapleton and Huntley*, 1995]. Thus, potential contamination of turbulent fluctuations in the inertial subrange by wave motions can be minimized by focusing on vertical velocities. Therefore, our velocity-based IDM estimates of bed shear stress were obtained only from spectra of the vertical components of flow following the methods of *Stapleton and Huntley* [1995].

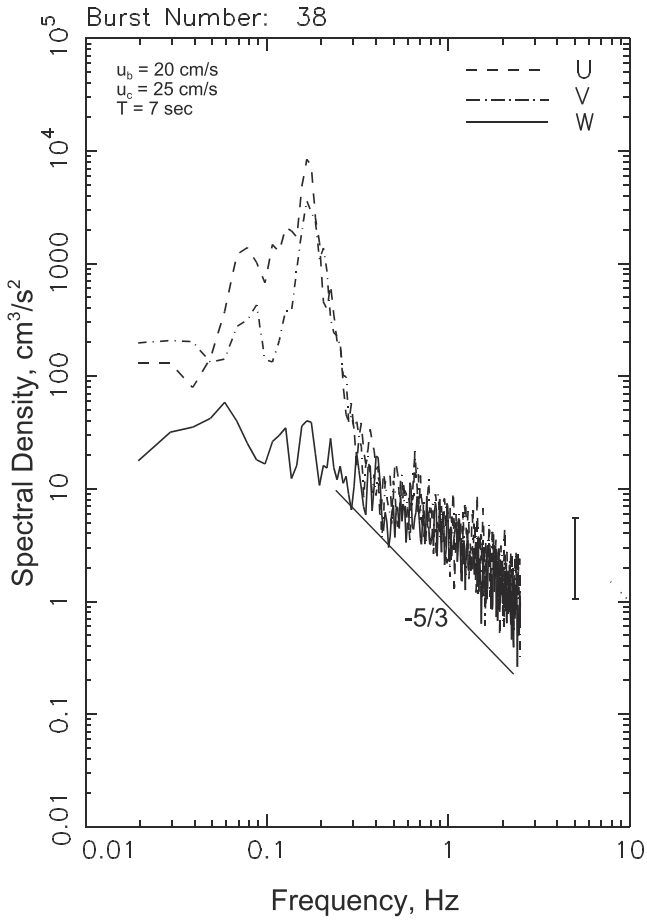

Figure 5. Representative spectra of horizontal and vertical turbulent velocities measured at 21 cm above the bed during a sampling burst for which the mean current velocity u_c, the near-bottom wave orbital velocity u_b and wave period T took on the indicated values. A −5/3 slope associated with the inertial subrange is indicated for comparison.

[29] Two different estimates were compared for the dominant flow speed, U, advecting turbulence past the instruments, (1) the standard burst-averaged velocity, u_c, and (2) a potentially appropriate root-mean squared (RMS) wave speed, u_b. The RMS wave speed was considered because waves may be the dominant advection velocity when the mean current is weaker than the wave orbital velocity [cf. *Lumley and Terray*, 1983; *Agrawal et al.*, 1992]. In estimating U for use with ABS, we used current velocities observed at the heights of the ADV and EMCMs and interpolated current velocities via a log linear fit of observed current velocities to heights where current observations were unavailable.

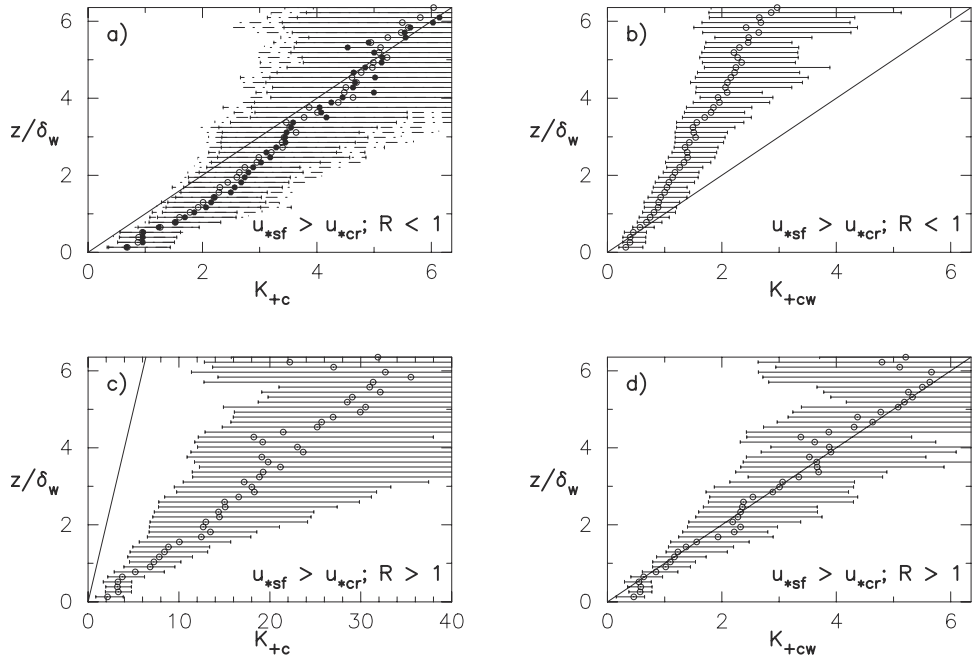

Figure 6. Inferred values of nondimensional eddy diffusivity K_+ as a function of relative elevation z/δ_w in flows for which u_{*sf} exceeds the critical value for initiation of motion u_{*cr}. Under strong currents (R < 1), eddy diffusivity was scaled with u_{*c} as shown in Figure 6a, while under weak currents, eddy diffusivities were scales with u_{*cw} as shown in Figure 6d. Figures 6b and 6d are plotted for comparison with Figures 6a and 6c with u_{*cw} and u_{*c}, respectively.

[30] In estimating bed shear stress from velocity, we consider the inertial spectral subrange to be bounded by lower wave number and frequency limits of $2\pi/z$ and $U(z)/z$, respectively [*Green*, 1992; *Stapleton and Huntley*, 1995], and by upper wave number and frequency limits of $2\pi/l_0$ and $U(z)/l_0$, respectively, where l_0 corresponds to the larger value of either the sensor averaging length or $U(z)/f_0$ for which f_0 is the sampling Nyquist frequency. For concentration, the practical upper limits are given by the same formulae, but the lower limiting frequency due to particle settling can be w_s/δ_s (see section 2.3), corresponding to a limiting wave number of $(2\pi/U)(w_s/\delta_s)$. For the ADV measurements (10 MHz, sampling 10 cm below probe), the averaging length is 1 cm; for ABS settings during the Duck deployment (a transmission half angle of 2.5°; 2 MHz), the length scale associated with the far-field sampling volume at 50 cm from the acoustic source is about 4.4 cm [c.f. *Hay*, 1991]. In general, flow speeds associated with marked sediment transport were 5 cm/s or greater for which lower-limiting inertial frequencies at 10-cm ab were thus of order 0.5 Hz. For a conservatively low sediment suspension height of δ_s = 10 cm, w_s/δ_s is of order 0.1 Hz, which is a less stringent constraint than $U(z)/l_0$. The upper limits of the inertial subrange in the ABS spectra typically corresponded to the Nyquist frequency of 2.5 Hz.

5. Results

5.1. Vertical Structure of Eddy Diffusivity From Suspended Sediment Concentrations

[31] In calculating dimensionless eddy diffusivity from suspended sediment concentrations, only cases for which $u_{*sf,gm}$ exceeded the critical value for initiation of motion u_{*cr} were considered; the number of bursts was thus 133 out of a total of 309. The selected bursts were grouped into strong and weak current cases according to a scaling parameter, R. The scaling parameter, R, is the ratio of the vertical advection velocity relative to the mean current at the top of the GM wave boundary layer [*Lee et al.*, 2002]. The vertical advection or "jet" velocity is defined as $(\eta/\lambda)u_b$ where η and λ are the modeled ripple height and ripple length [*Wiberg and Harris*, 1994], respectively. Periods with R < 1 correspond to strong current conditions for which the dominant suspension process is assumed to be turbulent diffusion associated with current-generated turbulence outside the wave boundary layer. There were 95 cases out of 133 with strong currents. These cases are shown with an asterisk in Figure 3c. Cases with R > 1 generally correspond to weak currents, but waves strong enough to suspend sediment from the bed. For R > 1, the dominant mechanism for initial sediment suspension is not near-bed turbulent diffusion, but wave-generated shedding vortices [*Lee et al.*, 2002]. There were 38 bursts for weak currents; these are shown with a cross in Figure 3c.

[32] Two pairs of median and quartile estimates of nondimensionalized eddy diffusivity K_+, defined in equation (2), are shown in Figure 6 as a function of relative height z/δ_w, where $\delta_w = 2u_{*cw,gm}/\omega$. Strong current cases are shown in Figures 6a and 6b, while weak current cases are presented in Figures 6c and 6d. For each of the two pairs, one of the pair was normalized by $u_{*c,gm}$ (i.e., K_{+c}, Figures 6a and 6c) and the other by $u_{*cw,gm}$ (i.e., K_{+cw}, Figures 6b and 6d). For comparison, K_+ normalized by $u_{*c,fit}$, where $u_{*c,fit}$ was determined by a best fit to observed current log-profiles (equation (3)), is also shown in Figure 6a by the solid circles

and dashed error bars. Note that nondimensionalized eddy diffusivities for each burst were interpolated into z/δ_w space before obtaining median and quartile estimates.

[33] In general, eddy diffusivity increases linearly with elevation and u_* to a height of about five times the wave boundary layer thickness δ_w. From Figures 6a and 6d, it is evident that eddy diffusivities for strong currents are scaled by u_{*c}, while eddy diffusivities for weak currents are scaled by u_{*cw}. For cases of strong currents, Figure 6a validates two fundamental assumptions necessary for the analytical development of the inertial dissipation method in sections 2.2 and 2.3: (1) $K \sim \kappa u_* z$ and (2) the equality of eddy diffusivities for mass and momentum. The first assumption further implies that stratification due to sediment suspension is dynamically unimportant. For cases of weak currents, Figure 6d suggests that wave-induced turbulence in the absence of currents often penetrates much higher than predicted by the classical value for δ_w. This further suggests the likelihood that the spectral methods developed above will be influenced by u_{*cw} if applied at $z < \sim 6\delta_w$ for cases of weak currents.

5.2. Bed Shear Stress Estimation From Velocity Measurements

[34] An example of spectral density of flow velocity during conditions of moderate wave energy is shown in Figure 5. The inertial subrange is clearly marked with a $-5/3$ slope. For the 90 sampling bursts considered here, the mean slope of the spectra of vertical velocities in the frequency range 0.3–2 Hz is -1.51 ± 0.16 SE (95% standard error). This value is only slightly smaller than the value of $-5/3$ expected for Kolmogorov scaling in the inertial subrange.

[35] Figure 7 shows ratios of IDM shear velocity estimates obtained from the w-velocity spectra ($u_{*c,ADV}$) and GM shear velocity estimates ($u_{*c,gm}$) as a function of $u_{*c,gm}/w_s$ and u_c/u_b. Estimates with (without) Huntley's correction given by equation (16), which used u_c as the advection velocity, are shown as open circles (solid squares) in Figure 7a. Under conditions of relatively small values of $u_{*c,gm}/w_s$ (<1), the spectral estimates of the shear velocity are consistently larger than those yielded by the GM model. The overestimation of $u_{*c,ADV}$ at small values of $u_{*c,gm}/w_s$ (<1) may be due to a poorly developed region of constant stress in the wave-current boundary layer for which the inertial dissipation method is not likely to apply. It is noted that a u_{*c} value of ~0.7 cm/s (equivalent $u_{*c,gm}/w_s \sim 1$) is similar to the minimum value ($u_{*c} = 0.8 \pm 0.2$ cm/s) that *Huntley* [1988] identified below which the inertial dissipation method is not likely to apply.

[36] In contrast, under conditions of intense flow for which $u_{*c,gm}/w_s$ is relatively large, spectral estimates using equation (13) subject to Huntley's correction are in good agreement (Figure 7a). The ratio of $u_{*c,ADV}$ to $u_{*c,gm}$ estimates has a mean value of 1.09 ± 0.05 SE (0.67 ± 0.04 SE) for with (without) the Huntley correction. Assuming Gaussian statistics, this mean value with the Huntley correction is not statistically different from unity. Overall, the significance of the Huntley correction is indicated by the consistent lack of agreement between GM and uncorrected IDM estimates.

[37] Estimates of Huntley-corrected $u_{*c,ADV}/u_{*c,gm}$ with u_c and u_b as the advection velocity are shown in Figure 7b as a function of u_c/u_b. The absolute differences, $\mathrm{abs}\left(u_{*c,ADV\_u_b} - u_{*c,ADV\_u_c}\right)/u_{*c,ADV\_u_b}$, between the two estimates with u_c and u_b are also shown in Figure 7b. The differences between two estimates are less than 10% during the periods when waves and currents have similar strength ($u_c/u_b > 0.7$). As the RMS wave velocity increases relative to the mean current ($u_c/u_b < 0.7$), the spectral estimates of shear stress with u_b reduce the overestimation significantly (up to 100 percent at the lowest ratio of u_c/u_b). Nonetheless, the estimates still significantly deviate from the actual shear stress. The systematic overestimate of shear velocity relative to $u_{*c,gm}$ for small u_c/u_b in Figure 7b may indicate the influence of u_{*cw} on $u_{*c,ADV}$ for cases such as those in Figure 6d where periodic wave-generated turbulence appears to penetrate well beyond the traditional wave boundary layer.

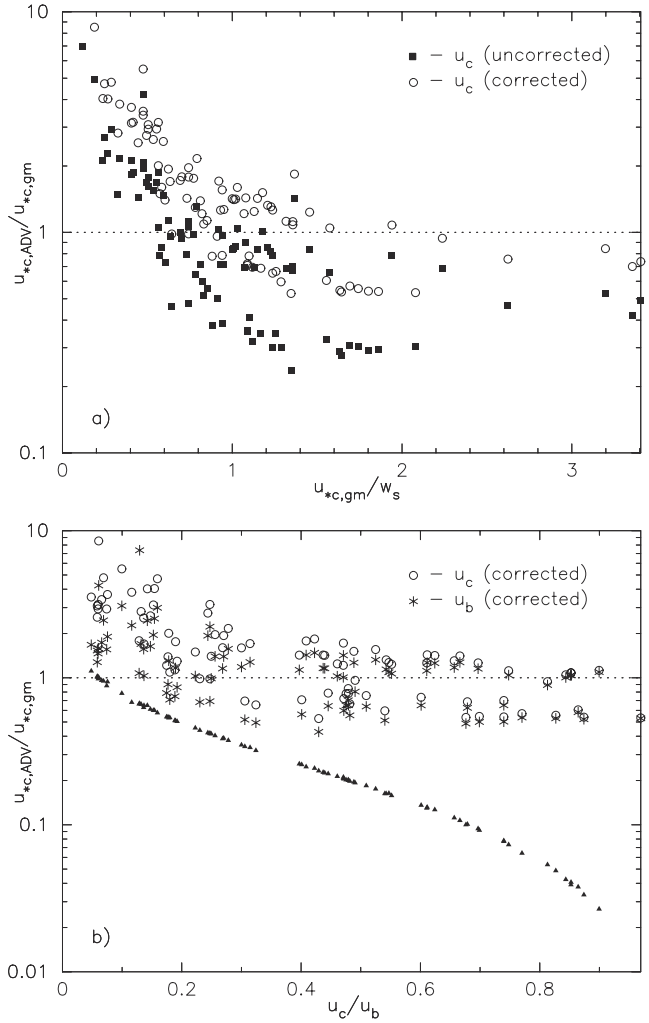

Figure 7. (a) Shear velocity estimates from the conventional inertial dissipation method as a function of $u_{*c,gm}/w_s$. The estimates are normalized by the corresponding $u_{*,gm}$. Circles and squares indicate estimates with and without Huntley's correction, respectively. Mean current velocity is used as the advection velocity. (b) Normalized shear velocity estimates by $u_{*,gm}$ as a function of u_c/u_b. Circles and asterisks indicate estimates with u_c and u_b as the advection velocity, respectively. Triangles represent the absolute difference between two estimates.

[38] Figure 8 shows a scatterplot of $u_{*c,gm}$ and $u_{*c,fit}$ versus Huntley-corrected $u_{*c,ADV}$ for large $u_{*c,gm}/w_s$ (>1). There exists a general one-to-one relationship between $u_{*c,ADV}$ and $u_{*c,gm}$ (and $u_{*c,fit}$). The mean values of absolute percent differences, 100* abs$(u_{*c}, \text{ADV} - u_{*c})/u_{*c}$, ADV, are 37 and 35% for $u_{*c,gm}$ and $u_{*c,fit}$, respectively.

5.3. Bed Shear Stress Estimation From Suspended Sediment Concentrations

[39] Shown in Figure 9 are representative spectral densities of suspended sediment concentrations as functions of frequency and elevation for the same burst portrayed in Figure 5, during which conditions corresponded to moderate wave energy. The mean slope of 133 spectra for which $u_{*sf,gm}$ exceeds the critical value for initiation of motion u_{*cr} at the height of EMCM2 (initially 38 cm ab) is -1.60 ± 0.05 SE. Note that the sediment concentration spectra is less dominated by the incident wave frequency than is u or v. This is consistent with our earlier inference that settling may prevent sediment concentration from resolving turbulent time-scales of order 0.2 Hz or less.

[40] Figure 10a shows ratios of IDM shear velocity estimates, which used u_c as the advection velocity, obtained from concentration spectra ($u_{*c,ABS}$) and GM shear velocity estimates ($u_{*c,gm}$) as a function of $u_{*c,gm}/w_s$. Cases for strong currents (R < 1) are shown as open circles and open squares, while cases for weak currents (R > 1) are shown as solid circles and solid squares. Cases for weak currents correspond to small values of $u_{*c,gm}/w_s$ (<1) and the spectral estimates of the shear velocity are consistently larger than those predicted by the GM model. Similar to $u_{*c,ADV}$, the overestimation $u_{*c,ABS}$ under weak currents may be due to a poorly developed region of constant stress or may indicate the influence of u_{*cw} on $u_{*c,ABS}$ for cases where periodic wave-generated vortex penetrates above the traditional wave boundary layer. For R < 1, estimates with (without) the Huntley correction are shown as open circles (open squares). Among these cases, the ratio of $u_{*c,ABS}$ to $u_{*c,gm}$ has a mean value of 0.87 ± 0.05 (0.60 ± 0.03) SE with (without) the Huntley correction. The Huntley correction is less severe for $u_{*c,ABS}$ than for $u_{*c,ADV}$ because the ABS bin examined was higher on average (24 cm ab during included bursts) than the ADV sensing volume (17 cm ab).

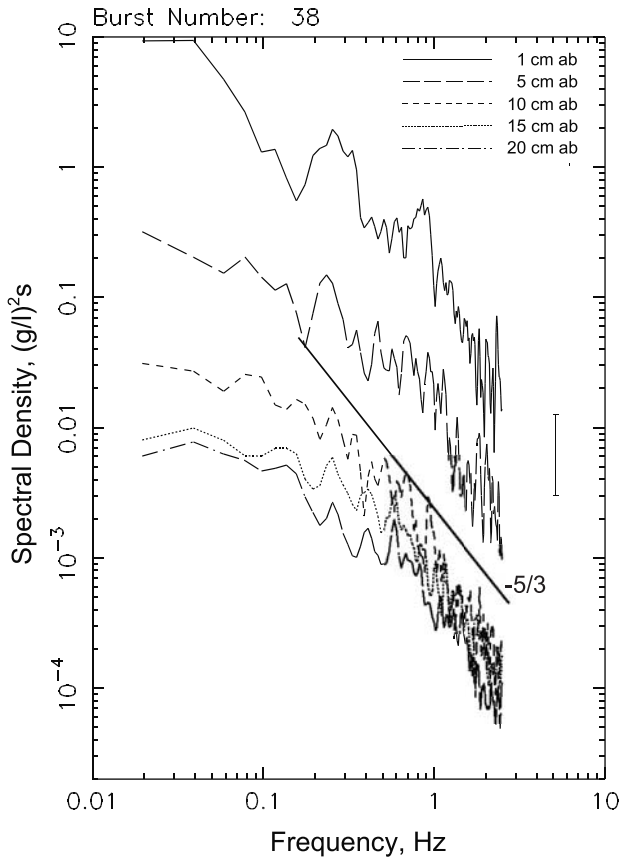

Figure 9. Spectra of turbulent sediment concentrations measured at 1-, 5-, 10-, 15- and 20-cm above the bed. A $-5/3$ slope associated with the inertial subrange is indicated for comparison.

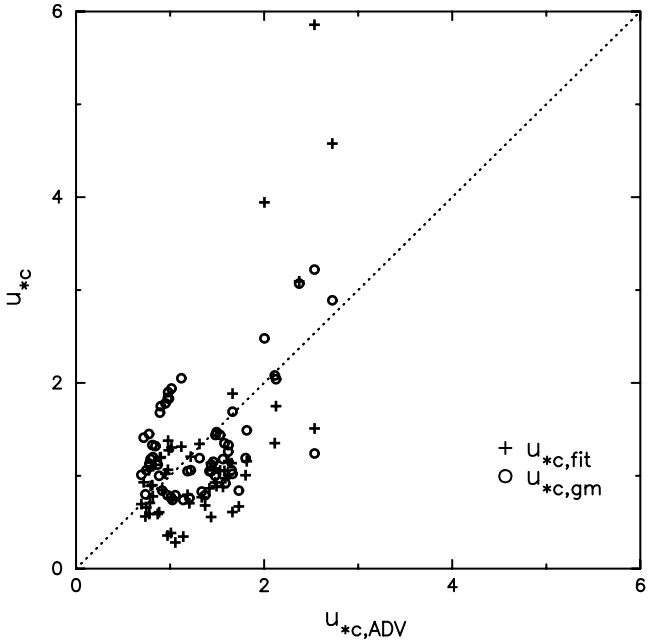

Figure 8. Scatterplot of $u_{*c,ADV}$ estimates against $u_{*c,gm}$. For comparison, $u_{*c,fit}$ is also shown in the figure.

[41] Estimates of Huntley-corrected $u_{*c,ADV}/u_{*c,gm}$ with u_c and u_b as the advection velocity are shown in Figure 10b as a function of u_c/u_b. The absolute differences, $\text{abs}\left(u_{*c,ABS\_u_b} - u_{*c,ABS\_u_c}\right)/u_{*c,ABS\_u_b}$, between the two estimates with u_c and u_b are also shown in Figure 10b. As seen for $u_{*c,ADV}$, the differences between two estimates of $u_{*c,ABS}$ decrease as waves and currents approach similar strength ($u_c/u_b > 0.7$).

[42] Figure 11 shows a scatterplot of $u_{*c,gm}$ and $u_{*c,fit}$ versus Huntley-corrected $u_{*c,ABS}$ (at the height of EMCM2) for R < 1. There exists a general one-to-one relationship between $u_{*c,ABS}$ and $u_{*c,gm}$ (and $u_{*c,fit}$). The mean values of absolute differences, $100*\text{abs}\left(u_{*c,ABS} - u_{*_c}\right)/u_{*c,ABS}$, are 34 and 43% for $u_{*c,gm}$ and $u_{*c,fit}$, respectively.

[43] Huntley-corrected $u_{*c,ABS}/u_{*c,gm}$ are shown in Figure 12 as a function of z/δ_w for the seven bursts with the largest predicted $u_{*c,gm}/w_s$. The advection velocity U needed to calculated $u_{*c,ABS}$ was chosen to vary as a function of height based on a log-fit to the observed velocity profile. The

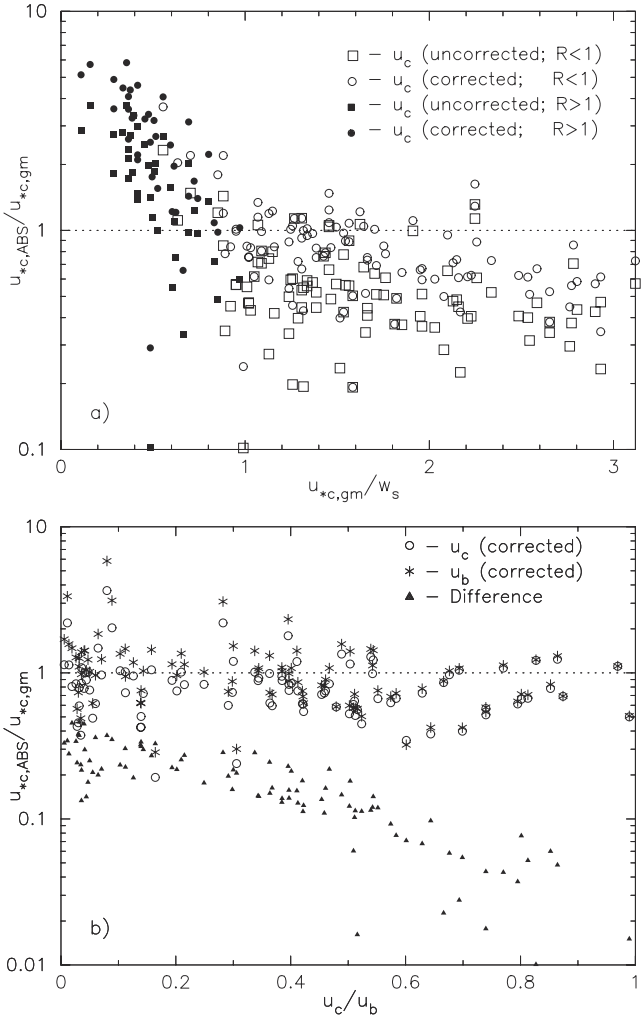

Figure 10. (a) Spectral estimates of the shear velocity based on concentrations of suspended sediment as a function of $u_{*c,gm}/w_s$. As in Figure 7, estimates are normalized by the corresponding, independent estimates from GM. Solid circles and solid squares are cases for R > 1, while open circles and open squares represent cases for R < 1. Circles and squares indicate estimates with and without Huntley's correction, respectively. Mean current velocity is used as the advection velocity. (b) Normalized shear velocity estimates by $u_{*,gm}$ as a function of u_c/u_b. Unlike Figure 10a, only cases for R < 1 are shown. Circles and asterisks indicate estimates with u_c and u_b as the advection velocity, respectively. Triangles represent the absolute difference between two estimates.

relative stability of the shear velocity estimate as a function of height supports the resiliency of $u_{*c,ABS}$ as well the presence of a constant stress layer. The increase in $u_{*c,ABS}/u_{*c,gm}$ very near the bed may indicate the influence of u_{*cw} on $u_{*c,ABS}$ within the wave boundary layer.

6. Discussion and Conclusions

[44] Acoustic Backscatter Systems provide powerful opportunities for noninvasive, high-resolution measurements of near-bed concentrations of suspended sediment.

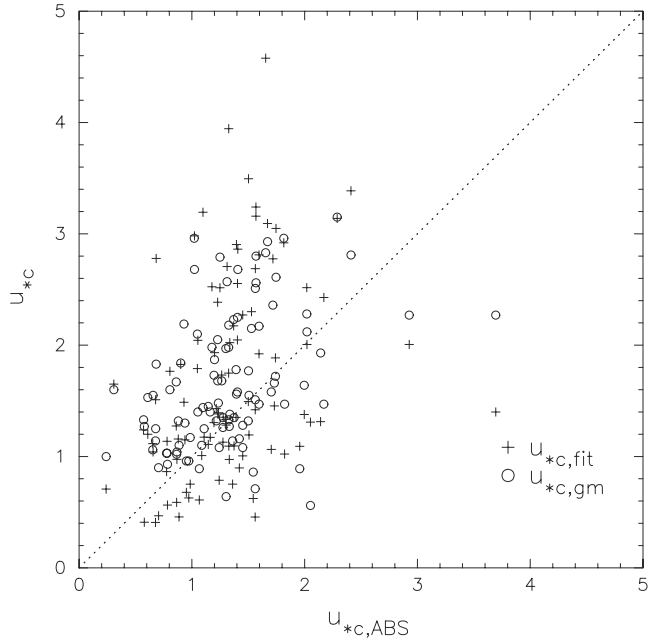

Figure 11. Scatterplot of $u_{*c,ABS}$ estimates against $u_{*c,gm}$. For comparison, $u_{*c,fit}$ is also shown in the figure.

We have examined time series of such measurements made in flows of combined waves and currents in a nearshore setting. Our study of these records was undertaken specifically with regard to an analysis of the potential for Kolmogorov scaling in spectra of passive tracers and, if such scaling were detected with confidence, to invert the analysis for estimates of the shear velocity of the transporting flows, a fundamental measure of flow intensity and the shear stress acting on the bed. In developing the inertial dissipation method for sediment concentration, we pursued an analogy between temperature and sediment concentration. But unlike temperature, a sediment particle cannot

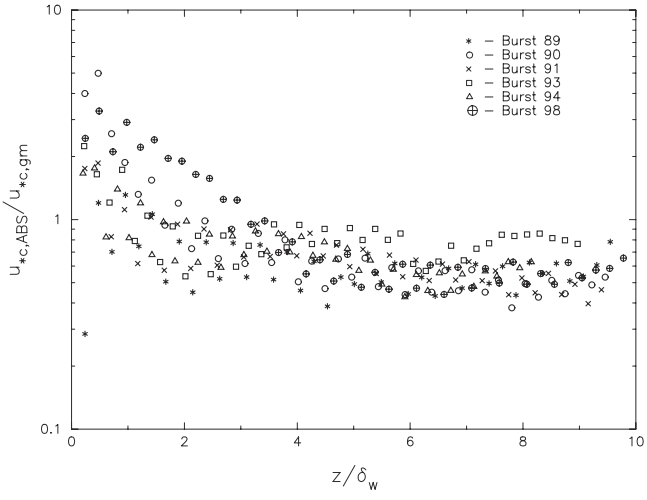

Figure 12. Spectral estimates of the shear velocity based on concentrations of suspended sediment as a function of relative elevation z/δ_w, and for flows for which $u_{*c,gm}/w_s > 3$. The estimates are normalized by the corresponding, independent estimates from GM.

resolve the shortest scales of turbulent fluid motion if its size or inertial response time is greater than the Kolmogorov microscales. For fine sand, these ultimate resolution limits are still much smaller than the sampling volumes and response times of field instrumentation typically applied to IDM.

[45] An analysis of the observed vertical structure of suspended sediment in terms of the conventional Rouse equation indicate an approximately linear relationship between eddy diffusivity of mass and height above the bed to elevations of at least 20 cm or equivalently, for the flow conditions observed, more than 4–5 times the wave boundary layer thickness. In particular, eddy diffusivity profiles were scaled with u_{*c} under strong currents. During weak currents, eddy diffusivity profiles were scaled with u_{*cw} and the vertical length scale extended about 5 times the classical wave boundary layer (Figure 6). The implication from these results is clear in that u_{*cw} must be used for weak currents even above the classical wave boundary layer in the Rouse-type equation as suggested by *Lee et al.* [2002] or an approach other than a diffusion model must be adopted for modeling sediment suspension under weak current conditions. Although the finding that eddy diffusivity follows a law-of-the-wall formulation equivalent to eddy viscosity is not surprising, its confirmation is fundamental to many transport models and indeed, underpins the following components of our analysis. Furthermore, the agreement between eddy diffusivity and an unstratified model for eddy viscosity during strong currents suggests that density stratification due to suspended sediment is not dynamically important.

[46] Dimensional analysis predicts and we observe Kolmogorov scaling in the inertial subrange, spanning frequencies of order 1 Hz, of power spectra of not only the flow itself, but also of concentrations of suspended sediment near the bed. The existence of $-5/3$ slope observed from concentration spectra within appropriate frequency bounds indicates that sand particles are effectively passive tracers of the turbulent motions of the suspending fluid, and thus can be used to study the structure and intensity of marine boundary layers over mobile beds. However, our earlier finding that u_{*cw} dominates the Rouse profile above the traditional wave boundary layer during weak current conditions suggests that the application of inertial dissipation technique for determining u_{*c} should be limited to cases with relatively strong currents. Furthermore, in relatively slow flows for which the shear velocity was less than about 0.8, spectral estimates of the flow shear velocity u_* were consistently larger than estimates inferred from GM. This is true for spectral estimates based on flow and sediment concentration observations alike.

[47] In applying this method to sufficiently intense mean flows, we find that at elevations between one and four times the thickness of the wave boundary layer, estimates of the shear velocity obtained from Kolmogorov scaling in the suspended sediment spectra consistently agree to within a factor of 2 with similar estimates from flow spectra and independent estimates from log-fits to the velocity profile as well as a widely used wave-current model [*Grant and Madsen*, 1986]. In addition, we note that an important aspect of conventional and new spectral analyses alike is the correction introduced by *Huntley* [1988] for observations made in near-bed flows characterized by insufficient separation of the scales of turbulence production and dissipation. The physical meaning of the correction is still unclear and the significance of this correction for suspended sediment concentration spectra is still a focus of study.

[48] Sources of the discrepancies up to a factor of 1 or 2 which do exist between the various estimates at this time include poor constraints on empirical model parameters (e.g., α_s introduced in equations (7) and (8), for which the value of 0.71 used here, well-established for scalar quantities, may not be strictly applicable for suspended sediment). Another source of significant error may be the characteristic settling velocity, w_s, which we set to be constant in time and with height above the bed. It is widely known that grading of sediment suspensions occur with elevation. More accurate, time and/or elevation-varying settling velocity may improve shear velocity estimates made in the future. We also acknowledge that the sampling rate of 5 Hz limited our resolution of the entire inertial subrange and thus our ability to confidently estimate shear velocity. In order to improve future estimation, a higher sampling rate is desirable.

[49] We have advanced here the development and application of a theory for spectral scaling in suspended sediment concentrations observed near the seabed. One application of the analysis focuses on an inversion of the theory for estimates of bed shear stress. We conclude that the approach shows significant promise. In this regard, we also note that if bed shear stress is known independently, one can use spectral scaling relationships for suspended sediment concentrations to estimate either the characteristic settling velocity (or equivalent sediment size) of the material in suspension or bed roughness, provided one or the other quantity is known. Such applications could provide powerful, new noninvasive tools to resolve, for example, frequently encountered discrepancies between the inferred caliber of materials comprising the bed and in suspension [e.g., *Lee et al.*, 2002]. Work on extending the analysis developed here is currently underway.

Notation

General

c'	fluctuating part of sediment concentration.
C	time-averaged sediment concentration (g/L).
d	suspended sediment particle size.
f	frequency.
f_o	Nyquist frequency.
k	wave number.
K	eddy diffusivity (cm^2/s).
K_+	dimensionless eddy diffusivity.
K_{+c}	dimensionless eddy diffusivity scaled with shear velocity due to currents.
K_{+cw}	dimensionless eddy diffusivity scaled with shear velocity due to the combined effect of waves and currents.
l_o	sensor averaging length.
R	scaling parameter.
Re_{cr}	critical Reynolds number.
U	dominant flow speed.
u	total instantaneous flow velocity.
u_b	root-mean squared wave speed.
u_c	time-averaged current velocity.

u_* characteristic shear velocity.
u_{*c} shear velocity due to currents.
u_{*cr} critical shear velocity.
u_{*cw} shear velocity due to the combined effect of waves and currents.
u_{*sf} skin-friction shear velocity.
$\hat{u}_{*c}$ shear velocity corrected by using the Huntley's correction.
w_s settling velocity of sediment grains (cm/s).
z height above the bed.
z_{cr} critical height above which measurements must be made to ensure an inertial subrange.
α_{ii} empirical constant in equations (6) and (9).
α_s empirical constant in equations (17) and (18).
δ_s characteristic sediment suspension height
δ_w thickness of wave boundary layer.
ε rate of TKE dissipation.
ε_s rate of dissipation of sediment fluctuation.
ϕ_{ii} TKE spectrum.
ϕ_s spectrum of sediment concentration.
η ripple height.
κ von Karman's constant.
λ ripple length.
ν kinematic viscosity of seawater.
ρ density of seawater.
τ_c bed shear stress associated with currents.
ω wave radian frequency.

Subscript

ABS shear velocity measured by inertial dissipation method of sediment concentration.
ADV shear velocity measured by inertial dissipation method of flow.
gm shear velocity measure by the GM wave-current interaction model.
u_b rms wave speed was used as characteristic advection velocity for IDM.
u_c time-averaged current speed was used as characteristic advection velocity for IDM.

[50] **Acknowledgments.** G.L. and W.B.D. gratefully acknowledge the support of the (UK) Atomic Energy Authority and the (UK) Natural Environmental Research Council. Participation by C.T.F. and field studies at Duck, N. C., were supported by the (U.S.) National Science Foundation.

References

Agrawal, Y. C., E. A. Terray, M. A. Donelan, P. A. Hwang, A. J. Williams III, W. M. Drennan, K. K. Kahma, and S. A. Kitaigorodskii, Enhanced dissipation of kinetic energy beneath surface waves, *Nature*, *359*, 219–220, 1992.

Bendat, J. S., and A. G. Piersol, *Random Data: Analysis and Measurement Procedures*, 566 pp., John Wiley, New York, 1986.

Birkemeier, W. A., H. C. Miller, S. D. Wilhelm, A. E. DeWall, and C. S. Gorbics, A user's guide to the Coastal Engineering Research Center's Field Research Facility, *Instruct. Rep. CERC-85-1*, Coastal Eng. Res. Cent., U.S. Army Corps of Eng., Vicksburg, Miss., 1985.

Dade, W. A., A. J. Hogg, and B. P. Bourdreau, Hydrodynamics of the benthic boundary layer, in *The Benthic Boundary Layer*, edited by B. P. Boudreau and B. B. Jorgensen, pp. 4–43, Oxford Univ. Press, New York, 2001.

Dietrichs, W. E., Settling velocity of natural particles, *Water Resour. Res.*, *18*, 1615–1621, 1982.

Glenn, S. M., and W. D. Grant, A suspended sediment stratification correction for combined wave and current flow, *J. Geophys. Res.*, *92*, 8244–8264, 1987.

Grant, W. D., and O. S. Madsen, The continental shelf bottom boundary layer, *Ann. Rev. Fluid Mech.*, *18*, 265–305, 1986.

Green, M. O., Spectral estimates of bed stress at subcritical Reynolds numbers in a tidal boundary layer, *J. Phys. Oceanogr.*, *22*, 903–917, 1992.

Gross, T. F., and A. R. M. Nowell, Spectral scaling in a tidal boundary layer, *J. Phys. Oceanogr.*, *15*, 496–508, 1985.

Gross, T. F., A. J. Williams III, and E. A. Terray, Bottom boundary layer spectral dissipation estimates in the presence of wave motions, *Cont. Shelf Res.*, *14*, 1239–1256, 1994.

Hay, A. E., Sound scattering from a particle-laden, turbulent jet, *J. Acoust. Soc. Am.*, *90*, 2055–2074, 1991.

Hay, A. E., and A. J. Bowen, Coherence scales of wave-induced suspended sand concentration fluctuations, *J. Geophys. Res.*, *99*, 12,749–12,765, 1994.

Hicks, B. B., and A. J. Dyer, The spectral density technique for the determination of eddy flux, *Q. J. R. Meteorol. Soc.*, *98*, 838–844, 1972.

Huntley, D. A., A modified inertial dissipation method for estimating seabed stresses at low Reynolds numbers, with applications to wave/current boundary layer measurements, *J. Phys. Oceanogr.*, *18*, 339–346, 1988.

Kim, S.-C., C. T. Friedrichs, J. P.-Y. Maa, and L. D. Wright, Estimating bottom stress in tidal boundary layer from Acoustic Doppler Velocimeter data, *J. Hydraul. Eng.*, *126*, 399–406, 2000.

Kundu, P. K., *Fluid Mechanics*, 638 pp., Academic Press, San Diego, Calif., 1990.

Lee, G., C. T. Friedrichs, and C. E. Vincent, Examination of diffusion versus advection dominated sediment suspension on the inner shelf under storm and swell condition, Duck, North Carolina, *J. Geophys. Res.*, *107*, 3084, doi:10.1029/2001JC000918, 2002.

Lee, T. H., and D. M. Hanes, Comparison of field observations of the vertical distribution of suspended sand and its prediction by models, *J. Geophys. Res.*, *101*, 3561–3572, 1996.

Lumley, J. L., Two-phase and non-Newtonian flows, in *Topics in Applied Physics*, vol. 24, edited by P. Bradshaw, pp. 507–527, Springer-Verlag, New York, 1977.

Lumley, J. L., and E. A. Terray, Kinematics of turbulence convected by a random wave field, *J. Phys. Oceanogr.*, *10*, 208–219, 1983.

McPhee, M. G., An inertial-dissipation method for estimating turbulent flux in buoyancy-driven, convective boundary layers, *J. Geophys. Res.*, *103*, 3249–3255, 1998.

Sharples, J., C. M. Moore, and E. R. Abraham, Internal tide dissipation, mixing, and vertical nitrate flux at the shelf edge of NE New Zealand, *J. Geophys. Res.*, *106*, 14,069–14,082, 2001.

Shaw, W. J., J. H. Trowbridge, and A. J. Williams III, Budgets of turbulent kinetic energy and scalar variance in the continental shelf bottom boundary layer, *J. Geophys. Res.*, *106*, 9551–9564, 2001.

Sheng, J., and A. E. Hay, Sediment eddy diffusivities in the nearshore zone, from multifrequency acoustic backscatter, *Cont. Shelf Res.*, *15*, 129–147, 1995.

Sleath, J. F. A., *Seabed Mechanics*, 355 pp., John Wiley, New York, 1984.

Sleath, J. F. A., Seabed boundary layers, in *The Sea*, vol. 9B, edited by B. Le Méhauté and D. M. Hanes, pp. 693–728, John Wiley, New York, 1990.

Smith, J. D., Modeling of sediment transport on continental shelves, in *The Sea*, vol. 6, edited by E. D. Goldberg et al., pp. 539–577, John Wiley, New York, 1977.

Smith, J. D., and S. R. McLean, Spatially averaged flow over a wavy surface, *J. Geophys. Res.*, *82*, 1735–1746, 1977.

Snyder, W. H., and J. L. Lumley, Some measurements of particle velocity autocorrelation functions in a turbulent flow, *J. Fluid Mech.*, *48*, 41–71, 1971.

Soulsby, R. L., A. P. Salkield, and G. P. Le Good, Measurements of the turbulence characteristics of sand suspended by a tidal current, *Cont. Shelf Res.*, *3*, 439–454, 1984.

Stapleton, K. R., and D. A. Huntley, Seabed stress determinations using the inertial dissipation method and the turbulent kinetic energy method, *Earth Surf. Processes Landforms*, *20*, 807–815, 1995.

Tennekes, H., and J. L. Lumley, *A First Course in Turbulence*, 300 pp., MIT Press, Cambridge, Mass., 1972.

Thorne, P. D., P. J. Hardcastle, and R. L. Soulsby, Analysis of acoustic measurements of suspended sediments, *J. Geophys. Res.*, *98*, 899–910, 1993.

Traykovski, P., A. E. Hay, J. D. Irish, and J. F. Lynch, Geometry, migration and evolution of wave orbital ripples at LEO-15, *J. Geophys. Res.*, *104*, 1505–1524, 1999.

Trowbridge, J. H., On a technique for measurement of turbulent shear stress in the presence of surface waves, *J. Atmos. Oceanic Technol.*, *15*, 290–298, 1998.

Vincent, C. E., and A. Downing, Variability of suspended sand concentrations, transport and eddy diffusivity under non-breaking waves on the shoreface, *Cont. Shelf Res.*, *14*, 223–250, 1994.

Vincent, C. E., and M. O. Green, Field measurements of the suspended sand concentration profiles and fluxes and of the resuspension coefficient γ_o over a rippled bed, *J. Geophys. Res.*, *95*, 11,591–11,601, 1990.

Vincent, C. E., and P. D. Osborne, Predicting suspended sand concentration profiles on a macro-tidal beach, *Cont. Shelf Res.*, *15*, 1497–1514, 1995.

Voulgaris, B., and J. H. Trowbridge, Evaluation of the Acoustic Doppler Velocimeter (ADV) for turbulence measurements, *J. Atmos. Oceanic Technol.*, *15*, 272–289, 1998.

Wiberg, P. L., and C. K. Harris, Ripple geometry in wave-dominated environments, *J. Geophys. Res.*, *99*, 775–789, 1994.

W. B. Dade, Department of Earth Sciences, Dartmouth College, Hanover, NH 03755, USA. (William.B.Dade@Dartmouth.edu)

C. T. Friedrichs, Virginia Institute of Marine Science, College of William and Mary, Gloucester Point, VA 23062, USA. (cfried@vims.edu)

G.-H. Lee, Korea Ocean Research and Development Institute, 1270 Sadong, Ansan 425-744, South Korea. (glee@kordi.re.kr)

C. E. Vincent, School of Environmental Sciences, University of East Anglia, Norwich, NR4 6TJ, UK. (c.vincent@uea.ac.uk)